Temperature Dependence of Excited State Proton Transfer in Ice

Pavel Leiderman, Anna Uritski, and Dan Huppert*

Raymond and Beverly Sackler Faculty of Exact Sciences, School of Chemistry, Tel Aviv University, Tel Aviv 69978, Israel

Received: January 18, 2007; In Final Form: March 29, 2007

We have studied the excited-state proton-transfer rate of four photoacids in ice as a function of temperature. For all four photoacids, we have found a non Arrhenius behavior of the proton-transfer rate constant, k_{PT}. d(ln k_{PT})/d(1/T) decreases as the temperature decreases. The average slope of ln(k_{PT})versus 1/T depends on the photoacid strength (pK*). The stronger the photoacid is, the smaller the slope. For the strongest photoacid 2-naphthol-6,8-disulfonate (2N68DS) the largest slope is 35 kJ/mol at about 270 K, and the smallest measured slope is about 8 kJ/mol at about 215 K. We propose that the temperature dependence of k_{PT} in ice at the temperature range 270 > T > 200 K can be explained as arising from contributions of two proton-transfer mechanisms over the barrier and tunneling under the barrier. At very low temperatures T < 200 K, the slope of ln(k_{PT}) versus 1/T increases again. At about 170 K, the proton-transfer rate is much slower than the radiative rate, and the deprotonated form of the photoacid cannot be detected in the steady-state emission spectrum. At lower temperatures, T < 200 K, the rate further decreases because of a limitation on the reaction caused by the restrictions on the H_2O hydrogen reorientations.

Introduction

The physics of ice[1−4] was studied extensively for many years. Electrical conductivity measurements by Eigen and co-workers[5] in the 1960s gave a large mobility 10−100 times larger than in water for the proton in ice. Further measurements showed that the proton low-frequency mobility in ice at about 263 K is about a factor of 2 smaller than in supercooled water[3,6,7]at the same temperature. Acid−base reactions in liquid aqueous solution are common in chemical and biological processes.[5,8−10] The study of proton reaction in the solid phase, and particularly in ice is rare and uncommon.[11,12] Intermolecular proton transfer in the excited state (ESPT) has been studied extensively in the liquid phase.[13−23] In the past decade we extensively studied the reversible photoprotolytic cycle of a photoacid. We used a proton-transfer model that accounts for the reversibility and for the diffusion assisted geminate recombination of the transferred proton with the deprotonated form of the photoacid.[20,22,23]

In the liquid phase of aqueous solution of several mild and strong photoacids, we found that the temperature dependence displayed as an Arrhenius plot of the proton-transfer rate constant exhibits a convex shape. k_{PT} of a commonly used photoacid 8-hydroxy-1,3,6-trisulfonate (HPTS) at the high-temperature range T > 280 K gave activation energy E_a of less than 5 kJ/mol. At lower temperatures including the supercooled region 260 < T < 280 K, the activation energy is not constant and increases as the temperature decreases. At about 260 K, the plot ln(K_{PT}) versus 1/T gives a slope of $E_a \sim 20$ kJ/mol.

In the past, we used a qualitative model for proton transfer that accounts for the unusual temperature dependence of ESPT process of photoacids in the liquid state.[24] The proton-transfer reaction depends on two coordinates; the first one depends on a generalized solvent configuration. The solvent coordinate characteristic time is in the range between the dielectric relaxation time τ_D and the longitudinal relaxation $\tau_L = (\epsilon_0)/(\epsilon_s)\tau_D$. The second coordinate is the actual proton translational motion along the reaction path. The model restricts the proton-transfer process to be stepwise. The proton moves to the adjacent hydrogen bonded solvent molecule only when the solvent configuration brings the system to the crossing point. Our simple model is along the lines of theories of nonadiabatic proton transfer.[25,26]

In a previous work[27] we extended the liquid-phase studies on the photoprotolytic cycle of a photoacid to the ice phase. In ice, in the high-temperature range 240 < T < 270 K, we found for the HPTS photoacid a nearly constant activation energy within an average value of about $E_a \sim 30$ kJ/mol.

In a more recent work, we extended the previous studies on proton transfer in ice and measured the photoprotolytic cycle of HPTS in water containing large concentrations of several electrolytes as well as in frozen water−methanol mixtures.[28] The Arrhenius plot of ln(k_{PT}) versus 1/T is nearly constant, and the activation energy of the proton transfer of an electrolyte solution is large, twice that in pure water $E_a \sim 60$ kJ/mol, while the activation energy of the proton-transfer rate in the solid phase of the water−methanol mixtures is somewhat lower than in pure water, $E_a \sim 28$ kJ/mol.

In a further study, we measured the photoprotolytic cycle of two photoacids HPTS and 2-naphthol-6,8-disulfonate (2N68DS) as a function of temperature in ice, in the presence of a small concentration (c < 30 mM) of an inert salt. The inert salt affects the geminate recombination between the transferred proton with the conjugate base of the photoacid. We used the Debye−Hückel theory to express the screening of the Coulomb electrical potential by the inert salt. We found that, in ice, the effective screening effect is rather large and the Debye−Hückel expression underestimates the measured effect. We explain the large screening in ice by the tendency to concentrate the impurities to confined volumes in order to minimize the ice crystal energy.[29]

* Corresponding author. E-mail: huppert@tulip.tau.ac.il. Phone: 972-3-6407012. Fax: 972-3-6407491.

10.1021/jp070424g CCC: $37.00
Published on Web 05/23/2007

Recently we have studied the kinetics of the reaction of a proton with a mild base in ice.[30] The proton was injected into the ice crystal by a proton-transfer reaction from an electronically excited photoacid. In aqueous liquid solution, mild bases react with the transferred proton with a large intrinsic rate constant. We used our diffusion assisted geminate recombination model based on the Debye−Smolochowski equation with an additional term to account for the proton scavenging by the base to fit the experimental data. In ice, the proton scavenging effect is rather large and the diffusion controlled reaction rate constant underestimates the measured proton scavenging effect in a wide range of concentrations and temperature.

In this contribution, we extended the previous studies of the temperature dependence of the proton-transfer rate in ice.[27,28,22,23] We carefully examined the proton-transfer rate constant at a much larger temperature range than previously reported: $270 > T > 240$ K. In this study, we focused our attention, in some of the cases, to much lower temperatures down to about 195 K. We used four photoacids with different pK^* values at room-temperature in water in the range $0.7 < pK^* < 2$. The photoacids in increasing order of their photoacidity are 2-naphtol-6-sulfonate (2N6S), 2-naphtol-8-sulfonate (2N8S), 8-hydroxypyrene-1,3,6-trisulfonate (HPTS or pyranine), and 2-naphtol-6,8-disulfonate (2N68DS). The main finding of this study is that the temperature dependence of proton-transfer rate constant, k_{PT}, is not constant, but depends on the temperature. We found for the four photoacids that the plot of $\ln(k_{PT})$ versus $1/T$ in the temperature range $210 < T < 270$ K is concave. At temperatures below 230 K, the temperature dependence of k_{PT} is rather small compared to its temperature dependence at 270 K. Below approximately 210 K, the temperature dependence of k_{PT} increases once again. At very low temperature, $T < 170$ K, we cannot observe the presence of the RO^- (the deprotonated) emission band. As in the liquid case, we propose that the temperature dependence of k_{PT} in ice can be described by two coordinates, the solvent coordinate and the proton translocation coordinate. The major contribution to the generalized solvent coordinate is the hydrogens' rotational motion creating D and L defects.[3] At the high-temperature region $T > 210$ K, the rate-limiting step is the actual proton transfer. At very low temperatures, the rate-limiting step is the solid restrictions on the H_2O hydrogen reorientations.

Experimental Section

Time-resolved fluorescence was acquired using the time-correlated single-photon counting (TCSPC) technique, the method of choice when sensitivity, a large dynamic range, and low-intensity illumination are important criteria in fluorescence decay measurements.

For excitation, we used a cavity dumped Ti:sapphire femtosecond laser, Mira, Coherent, which provides short, 80 fs, pulses of variable repetition rate, operating at the SHG and the THG frequencies, over the spectral ranges 380−400 and 250−290 nm with the relatively low repetition rate of 500 kHz. The TCSPC detection system is based on a Hamamatsu 3809U, photomultiplier, and Edinburgh Instruments TCC 900 computer module for TCSPC. The overall instrumental response was about 35 ps (fwhm). Measurements were taken at 10 nm spectral width. The observed transient fluorescence signal, $I(t)$, is a convolution of the instrument response function (IRF), $I_0(t)$, with the theoretical decay function. The excitation pulse energy was reduced by neutral density filters to about 10 pJ. We checked the sample's absorption prior to and after time-resolved measurements. We could not find noticeable changes in the absorption spectra due to sample irradiation.

Steady-state fluorescence spectra were taken using a FluoroMax (Jobin Yvon) spectrofluorimeter and a miniature CCD spectrograph CVI MS-240. The HPTS (of laser grade), 2-naphthol-6,8-disulfonate (2N68DS), and 2-naphthol-6-sulfonate were purchased from Kodak, and 2-naphthol-8-sulfonate was purchased from TCI (Japan). Perchloric acid, 70% reagent grade, was purchased from Aldrich. For steady-state fluorescence measurements, we used photoacid solutions of $\sim 2 \times 10^{-5}$ M. For transient measurements, the sample concentrations were between 2×10^{-4} and 2×10^{-5} M. Deionized water had resistance >10 MΩ. Methanol of analytical grade was from Fluka. D_2O 99% was purchased from BDH. All chemicals were used without further purification. The solution pH was about 6.

The HPTS fluorescence spectrum at room temperature consists of two structureless broad bands (~40 nm fwhm). At temperatures below $T < 150$ K, the ROH emission band exhibits a distinctive vibration structure. The emission band maximum of the acidic form (ROH*) and the alkaline form (RO^-*) in water are at 445 and 510 nm, respectively. At 435 nm, the overlap of the two luminescence bands is rather small. The contribution of the RO^-* band to the total intensity at 435 nm is less than 0.2%. To avoid overlap between contributions of the two species, we mainly monitored the ROH* fluorescence at 435 nm.

The 2N68DS, 2N6S, and 2N8S fluorescence spectrum consists of two structureless broad bands (~40 nm fwhm). The emission band maximum of the acidic form (ROH*) in water is at about 370 nm, and that of the alkaline form (RO^-*) is at 440 nm for 2N6S and 2N8S and 470 nm for 2N68DS. At 370 nm, the overlap of the two luminescence bands is rather small. To avoid overlap between contributions of the two species, we mainly monitored the ROH* fluorescence at 375 nm.

The temperature of the irradiated sample was controlled by placing the sample in a liquid N_2 cryostat with a thermal stability of approximately ±1.5 K.

In the solid phase, the photoacids tend to aggregate, and as a consequence, the luminescence intensity in frozen samples is strongly reduced. The net result is an unreliable time-resolved emission measurement in the ice phase, of both the acid (ROH*) and base (RO^-*) forms. The aggregation problem of the photoacids in the ice phase was unnoticed when a small amount of methanol, ~1% mole fraction, was added to the solution.

Ice samples were prepared by first placing the cryogenic sample cell, for about 20 min, at a temperature of about 273 K. The second step involved a relatively rapid cooling (10 min) to a low temperature. The sample subsequently freezes within 5 min. To ensure ice equilibration prior to the time-resolved measurements, the sample temperature is kept constant for another 30 min.

Reversible Diffusion-Influenced Two-Step Proton-Transfer Model. In this model,[20,22,23] the photoprotolytic cycle can be subdivided into the two consecutive steps of reaction and diffusion. In the reactive step, a rapid proton transfer creates a solvent-stabilized ion pair. This is followed by a diffusive stage, when the proton and RO^- withdraw from each other due to their thermal random motion. The reverse process is a geminate recombination of the proton with the RO^- to reform the excited photoacid ROH*.

Mathematically, one considers the probability density, $p(r, t)$, for the RO^-*, H^+ pair to separate to a distance r by time t after excitation. The observed (normalized) signals from the excited acid ROH* and the RO^- anion correspond to the probability, to find the ROH* form $P(t)$, and the survival

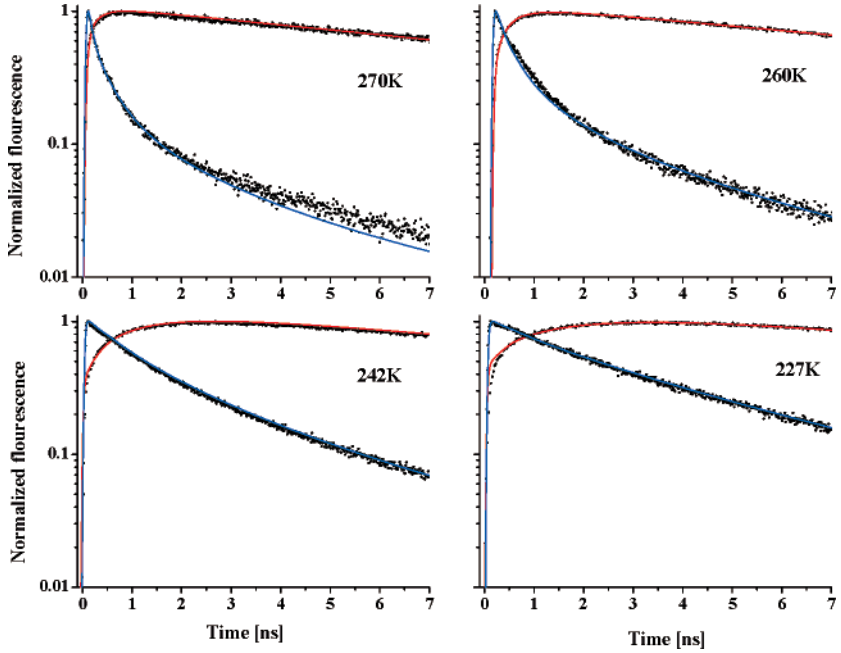

Figure 1. Time-resolved emission of 2N68S measured at 385 nm (ROH band) and 470 nm (RO^- band) in methanol-doped ice at 270, 260, 242, 227 K. Solid line is the calculated fit using the geminate recombination model.

probability of the separated pair, $S(t)$, which is also the probability to find the excited photoacid in its RO^- form

$$S(t) \equiv 4\pi \int_a^\infty p(r, t) r^2 \, dr \tag{1a}$$

$$P(t) = 1 - S(t) \tag{1b}$$

The separated pair at time t, $p(r,t)$ is assumed to obey a spherically symmetric Debye−Smoluchowski equation (DSE) in three dimensions, which is coupled to a kinetic equation for $P(t)$, which serves as the boundary condition for the differential equation.[20,22,23]

Results

Figure 1 shows the time-resolved emission of both the protonated ROH* and the deprotonated RO^-* forms of the strong photoacid 2N68DS measured by time-correlated single photon counting at several temperatures. The intensity of the fluorescence decay is displayed on a semilog plot. In general, the ROH decay of a photoacid is composed of two components. The short time component is fast and decays nearly exponentially. The fast component decay rate is mainly determined by the proton-transfer rate constant, k_{PT}. The longer time decay component is nonexponential, and it arises from the geminate recombination of the transferred proton to the medium back with the excited RO^-. The asymptotic long-time of the ROH fluorescence intensity I_f^{ROH} multiplied by the $\exp(t/\tau_f)$ (where τ_f is the radiative lifetime) obeys a power law of $t^{-3/2}$. We used the reversible diffusion influenced proton-transfer model[20,22,23] to fit the time-resolved emission curves of both ROH* and RO^-*. The calculated model fit is shown as a solid curve. As seen in the figure, the fits are rather good. We used the same parameters for the fit of the ROH and RO^-forms. From the best fit we extracted the parameters that control the dynamics of the excited state. The parameters are the radiative rates of ROH* and RO^-*, the proton-transfer rate constant k_{PT}, and the geminate recombination rate constant k_r. An important additional parameter in the photoprotolytic process is the proton diffusion constant in ice that also strongly depends on the temperature. We estimate that for the stronger photoacids 2N68DS and HPTS the proton-transfer rate constant is determined by the GR model with an error of about 10% at the high-temperature region $T >$ 240 K. At lower temperatures, the error increases for two reasons. The first reason is the limited time window of observing a molecule in the excited state which is determined by the excited-state lifetime of both ROH and RO^-. At about 240 K, the rate constant k_{PT} for HPTS is about that of the radiative rate k_0. While k_0 is almost insensitive to the temperature, k_{PT} strongly depends on it, and below 240 K the values of k_{PT} are lower than the values of k_0. The second reason for a larger error of k_{PT} at low temperatures concerns the large decrease of the ratio between the relative intensities of the fast component and the long components of the ROH decay. At high temperature, the fluorescence tail intensity is rather small compared to the fast component from which we determine k_{PT}. At low temperature, the relative tail intensity is large and increases as the temperature decreases.

At low enough temperature, the fluorescence tail coalesces with the short time component as well as with the radiative rate. At this limiting case, the fitting procedure provides an ambiguous set of the parameters, k_{PT}, k_r, and D. At low temperature, we use the steady-state emission spectra of ROH and RO^- to provide indirect information on the photoprotolytic process. We used the following relations of Weller[10] to extract an additional estimate for $k_{PT}(T)$.

The relative fluorescence of the ROH band is given approximately by

$$\frac{\Phi(T)}{\Phi_0} = \frac{k_0}{k_{PT}(T) + k_0} \tag{2}$$

where k_0 is the radiative rate of ROH, and Φ_0 is the fluorescence quantum yield of ROH in the absence of proton transfer. At room temperature, the proton-transfer rate constant of HPTS is $k_{PT} \simeq 10$ ns^{-1}, while $k_0 = 0.19$ ns^{-1} is temperature independent. As the temperature decreases, Φ/Φ_0 increases. At

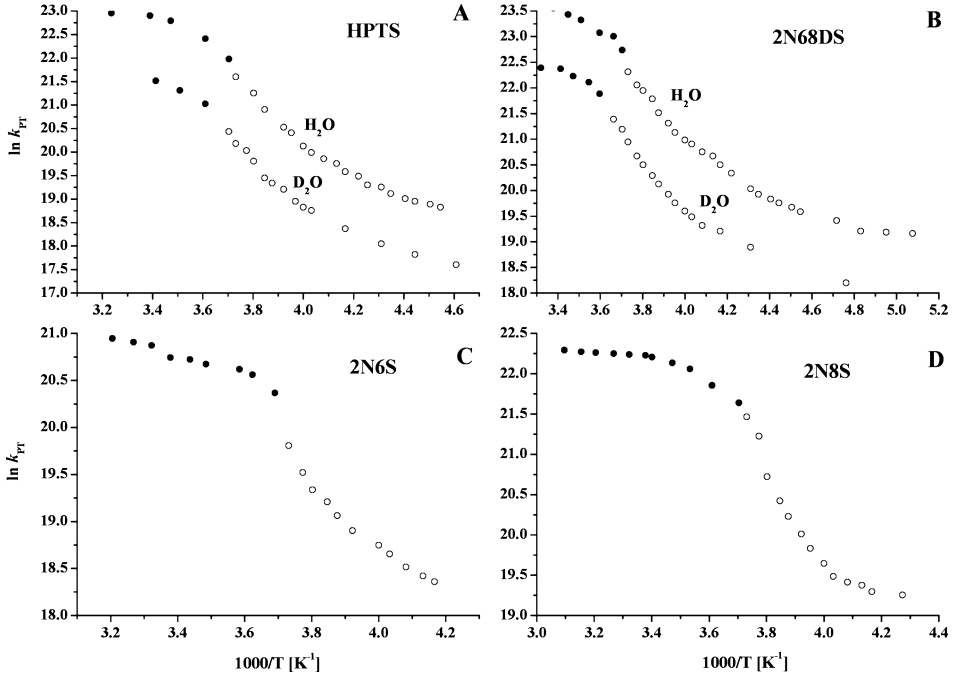

Figure 2. Plot of ln(k_{PT}) versus 1/T: (A) HPTS in H_2O and D_2O, (B) 2N68DS in H_2O and D_2O, (C) 2N6S in pure water, (D) 2N8S in pure water H_2O.

about 230 K, $k_{PT} \sim k_0$, and the fluorescence intensity of ROH is about 0.5 times that at very low temperatures $T < 100$ K where $k_{PT} \ll k_0$. The relative fluorescence of the RO^{-}* when the ground state of ROH is excited is given by

$$\frac{\Phi'(T)}{\Phi'_0} = \frac{k_{PT}(T)}{k_{PT}(T) + k_0} \tag{3}$$

Φ' is the fluorescence quantum yield of the RO^- form when the ROH form is excited, and Φ'_0 is the quantum yield when the RO^- form is excited. The fluorescence intensity ratio between the ROH and RO^- bands Φ'/Φ is given by

$$\frac{\Phi'(T)}{\Phi(T)} = \frac{k_{PT}(T)}{k_0} \tag{4}$$

Figure 2 shows an Arrhenius plot of ln(k_{PT}) versus 1/T for the four photoacids. All four plots show a similar concave shape of the Arrhenius plot of ln(k_{PT}) in ice. The proton-transfer rate constant of four photoacids in ice at a temperature close to the melting point are about a factor of 1.5 ± 0.2 smaller than the rate constant in supercooled liquid at the same temperature. Thus, solid ice is a good media for the ESPT process, almost as good as the liquid state. In comparison, the ground state proton-transfer rate constant in methanol as a solvent of acid−base reaction is lower by about 4 orders of magnitude than in water.[8] Since the excited-state lifetime of the ROH form is a few nanoseconds, and in water the proton-transfer rates of these photoacids are between 1×10^9 and 2×10^{10} s^{-1}, the excited-state proton transfer in methanol cannot be observed excluding the strongest photoacid used in this study, 2N68DS.

As seen in Figure 2, the temperature dependence of ln(k_{PT}) is not constant as expected only from a usual activated process. The lower the temperature, the smaller d[ln(k_{PT})]/d(1/T). We used a differentiation procedure given in a previous paper[27] to provide the rate of change of ln(k_{PT}) with respect to 1/T in units of kJ/mol. Figure 3 shows the change in the "activation" energies

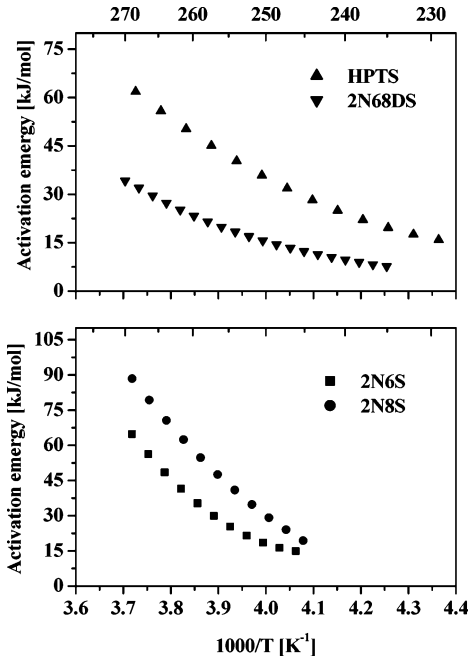

Figure 3. Activation energies of the HPTS, 2N68DS (upper figure) and 2N6S, 2N8S (lower figure) with temperature.

of the four photoacids with temperature. The photoacids with the smallest temperature dependence of ln(k_{PT}) is the 2N68DS (pK* ≈ 0.7) which is also the strongest of the four photoacids used in this study. The "activation" energy at the freezing point is about 37 kJ/mol, and it decreases steadily to about 8 kJ/mol at about 230 K. The activation energies of HPTS (pK* ≈ 1.3), 2N8S (pK* ≈ 1.6), and 2N6S (pK* ≈ 2) at the freezing point are larger by about a factor of 2 than that of 2N68DS. The rate of change in the activation energy of the two weaker photoacids 2N6S and 2N8S (the second derivative) is slightly larger than for HPTS.

Discussion

In a previous paper,[27] we focused our attention on the excited-state proton transfer in ice of only one photoacid, the well-known HPTS (pK^* = 1.35). Later on, in our recent papers,[29,30] we also added some information on k_{PT} of a stronger photoacid 2N68DS (pK^* = 0.7). We found in a limited range of temperatures, 268−240 K, that the proton-transfer rate constant, k_{PT}, of both photoacids decreases as a function of $1/T$ approximately as an activated process obeying an Arrhenius law (constant slope) with activation energies around 30 kJ/mol. In our current study, we extended our previous studies in two directions. The first one was toward increasing the ice temperature range; i.e., we lower the temperature as much as possible. The second direction was to look for more photoacid molecules and by this to say something more general on the temperature dependence of photoacids in ice.

The main finding of this study is that the plot of $\ln(k_{PT})$ as a function of $1/T$ on a large temperature range of about $\Delta T = 70$ K clearly shows that the slope of such a plot is not constant and tends to decrease at low temperatures. The concave shape of $\ln(k_{PT})$ versus $1/T$ in ice samples is found for all four photoacid. Unlike in ice, in the liquid state, the plot of $\ln(k_{PT})$ versus $1/T$ of a large number of photoacids is convex. At high-temperature $T > 280$ K, the slope is small. For strong photoacids, it is about 5 kJ/mol, while for 2-naphthol (pK^* = 2.7) the weakest photoacid the slope was about 12 kJ/mol at room temperature.[31] At lower temperatures, $T < 280$ K, the slope of $\ln(k_{PT})$ as a function of $1/T$ increases as the temperature decreases. In the case of HPTS in cold water $T \sim 273$ K and supercooled water $T \sim 268$ K, the activation energy is much larger than at the high-temperature regime, and at 268 K it is about 20 kJ/mol. In ice samples at about 270 K the value of the proton-transfer rate constant, k_{PT}, of all four acids we measured in the current study, 2N68DS (p$K^* \approx 0.7$), HPTS (p$K^* \approx 1.3$), 2N8S (p$K^* \approx 1.6$), 2N6S (p$K^* \approx 2.0$), is by about a factor of 1.5 smaller than in supercooled liquid at the same temperature. In HPTS the value of the rate constant k_{PT} in the liquid state drops from about 10 ns^{-1} at 295 K to about 6.7 ns^{-1} at about 270 K while the value of k_{PT} in ice at 270 K is about 4.5 ns^{-1}.

There are several plausible mechanisms that contribute to the proton-transfer rate in ice. In liquid solution,[24,32] the temperature dependence of the proton-transfer constant was explained as a combination of two dynamic processes that occur at two orthogonal coordinates, the solvent and the proton. The first process is a motion along a generalized solvent reorganization coordinate toward the solvent activated configuration. At the solvent activation configuration, the proton moves along the proton coordinate to form the product $RO^{-*} + (H_3O^+)(H_2O)_n$ where n is the number of water molecules in the solvation shell of the hydronium ion H_3O^+. For strong photoacids in the liquid state in the low-temperature regime, the rate-limiting step is the solvent motion while at the high-temperature regime the proton motion to form the product is the rate-limiting step. The reaction takes place only when the solvent reaches the configuration of the activated region.

Ice I is considered as an ordered hexagonal crystal structure with respect to the oxygen atom positions. The hydrogen position tends to be between two oxygens along the line connecting two oxygens.[2,3] In contrast to the order in the oxygens' position in pure ice at high temperature, a fraction of about 10^{-7} of the hydrogens are incorrectly ordered. According to Jaccard theory,[33] the electrical properties of ice are largely due to two types of defect within the crystal structure which allow protons to move along the hydrogen bonds under the influence of an external field. Ion defects are produced when a proton moves from one end of the oxygen−oxygen bond to the other, thus creating a H_3O^+, OH^- ion pair. Conduction is then possible by means of successive proton jumps. Bjerrum defects are orientational defects caused by the rotation of a water molecule to produce either an oxygen−oxygen bond occupied with two hydrogens (D-defect) or a bond with no hydrogens (L-defect). A series of successive rotations will produce conduction. Neither process alone can explain the dc conduction. For example, the movement of a H_3O^+ ion sets the protons in such a position that no more H_3O^+ ions may subsequently follow the same path. A similar effect occurs with Bjerrum defects. However, if an ion defect is followed by a Bjerrum defect then the protons will be reset into their original positions and the conduction pathway unblocked. In ice, the analogue to the liquid solvent reorganization motion accompanied with proton-transfer process is a restricted rotation of 120° of the hydrogens while the oxygen positions are fixed in a hexagonal structure and thus serve as a pivot to the hydrogen orientation motion. The mechanism of excess proton transfer in ice was investigated by Ohmine and co-workers[34] using the QM/MM method. By analyzing the potential surface, the normal modes, and the interaction between the excess proton and the defects, they propose that the ejected proton is localized in an L-defect in ice.

It is plausible that hydrogen rotation is a prerequisite step prior to the proton translocation from the protonated excited photoacid ROH* to a nearby water molecule. In a preliminary study, we observed the excited-state solvation dynamics of coumarin 343 (C343) in ice. In ice at 247 K using time-resolved emission technique with a time resolution of about 20 ps, we found a red shift of the emission band by about 600 cm^{-1} that occurs at an average solvation time $\langle\tau_s\rangle$ of about 60 ps. At about 190 K the average solvation time $\langle\tau_s\rangle$ increased by about a factor of 30 to about 2 ns. At about 170 K the dynamic red band shift is not observed within the time window limited by the 4 ns lifetime of C343. The steady-state emission spectrum of C343 in ice as a function of temperature shows a distinct blue shift upon temperature decrease. Below 170 K the band position is fixed.

The coumarin 343 solvation dynamics and the temperature dependence of the steady-state spectrum can be qualitatively related to the proton transfer of photoacids in ice and its temperature dependence. In the excited state, the solvation energy in ice is gained when the hydrogen atoms of near by water molecules rotate to accommodate the excited-state charge distribution. Proton transfer from the excited state will occur only after hydrogen atom rotation to bring the system along the generalized solvent coordinate to the activated region.

Below 195 K, the proton-transfer rate constant from 2N68DS is smaller than the excited-state radiative decay rate 0.11 ns^{-1}. As mentioned above, it is quiet difficult to measure accurately the proton-transfer rate from time-resolved emission measurements when $k_{PT} \leq k_0$, (where k_0 is the radiative rate). The main reason is that the radiative rate limits the time window of the measurements of small values of k_{PT}. The second difficulty arises from the large effective proton geminate recombination rate at low temperature. It increases the amplitude of the time-resolved emission longtime tail and thus interferes at slow proton-transfer rate with the initial fluorescence decay that basically enables us to separate the two processes and hence determine the proton-transfer rate.

Steady-state emission spectra of a photoacid excited at the ROH band can provide additional indirect information on the rate of the proton-transfer process and on solute−solvent

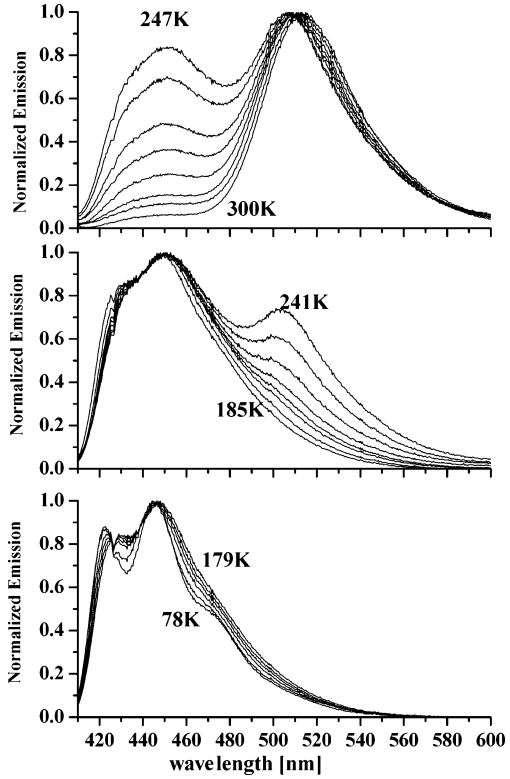

Figure 4. Steady-state emission spectrum of HPTS in pure water at various temperatures.

interaction. Figure 4 shows the emission spectra of HPTS in H_2O at various temperatures. We split the figure to three regions. Figure 4a shows the high-temperature region where the lowest temperature is at 247 K. For HPTS in H_2O at about 240 K, the value of the proton-transfer rate constant is about that of the radiative rate constant. As seen in the figure, the ROH band intensity in H_2O increases from about 3% with respect to the RO^- band intensity in the liquid state at a temperature of 293 K to be larger than the RO^- at 247 K.

Figure 4b shows the spectra at the intermediate temperature range. In this range, the radiative rate k_0 is larger than the proton-transfer rate constant k_{PT}. At the lowest temperature, 185 K, the RO^- band is still seen as a very small increase of the emission intensity at around 500 nm. In the third temperature range, $T < 179$ K, the only emission band seen in this figure is that of the ROH band. The proton-transfer rate constant $k_{PT} \ll k_0$, and only the fluorescence tail of the ROH band is seen at about 500−510 nm. The ROH emission spectrum at temperature below 180 K shows a distinctive vibration progression. We found similar results for a deutarated sample. The only differences are the relative intensities of the two bands I_{ROH}/I_{RO^-}, because of a slower deuteron transfer rate.

We fitted the ROH emission band of HPTS with four vibronic bands where the 0−0 band is positioned at 23400 ($T \approx 80$ K) and the vibronic spacing is about 1200 cm^{-1}. The intensity ratio of the vibronic peaks is 1, 1, 0.37, and 0.075, respectively. All four vibronic bands have about the same width and asymmetry. We used the log-normal function[35] to fit each individual vibronic band. At the lowest temperature range, the bandwidth is 1150 cm^{-1}, and each band is well separated from its neighbor. The bandwidth and position start to change only above 125 K. Figure 5 shows the red shift of the peak position of the ROH second vibronic band and the increase in its bandwidth as a function of temperature. As seen in the figure, the band shifts to the red, and the bandwidth increases monotonically with temperature

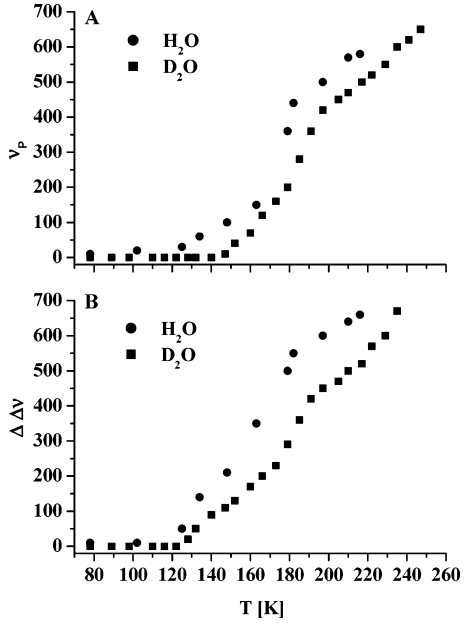

Figure 5. (A) Red shift of the ROH band peak. (B) The increase in bandwidth of ROH HPTS in H_2O and D_2O at various temperatures.

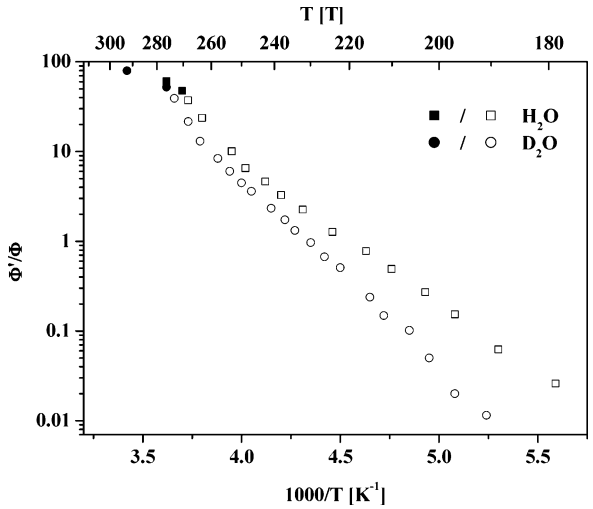

Figure 6. Φ'/Φ of HPTS in H_2O and D_2O at various temperatures.

increase. At about 180 K, the bandwidth and the peak position of ROH spectrum of HPTS exhibit a large change. The change in the ROH spectrum is accompanied by the appearance of the RO^- band. We interpret the large changes in the HPTS spectra at about 180 K as the ability of the H_2O hydrogens to rotate by 120° next to the HPTS molecule. Once the rotation time τ_{rot} is shorter than τ_{rad}^{ROH} the excited-state proton-transfer process starts to be effective and the RO^- band appears in the steady-state spectra.

From the steady-state emission spectra, we estimate the proton-transfer rate constant at various temperature using Weller's equations[10] (see eq 4). Figure 6 shows a semilog plot of (k_{PT}) of HPTS in H_2O and D_2O versus $1/T$ deduced from the steady-state emission spectrum. In the high-temperature region, the values of k_{PT} deduced from the time-resolved emission and the steady-state spectra are quite similar. At the intermediate temperature range $240 > T > 210$ K, the values of k_{PT} from steady-state emission are smaller than the values obtained from the time-resolved emission. As mentioned above, when $k_{PT} \leq k_0$ it is quite difficult to deduce k_{PT} from the time-resolved emission fitting by the GR model, since the contribution of the long time tail overlaps with the initial fast decay. On the other

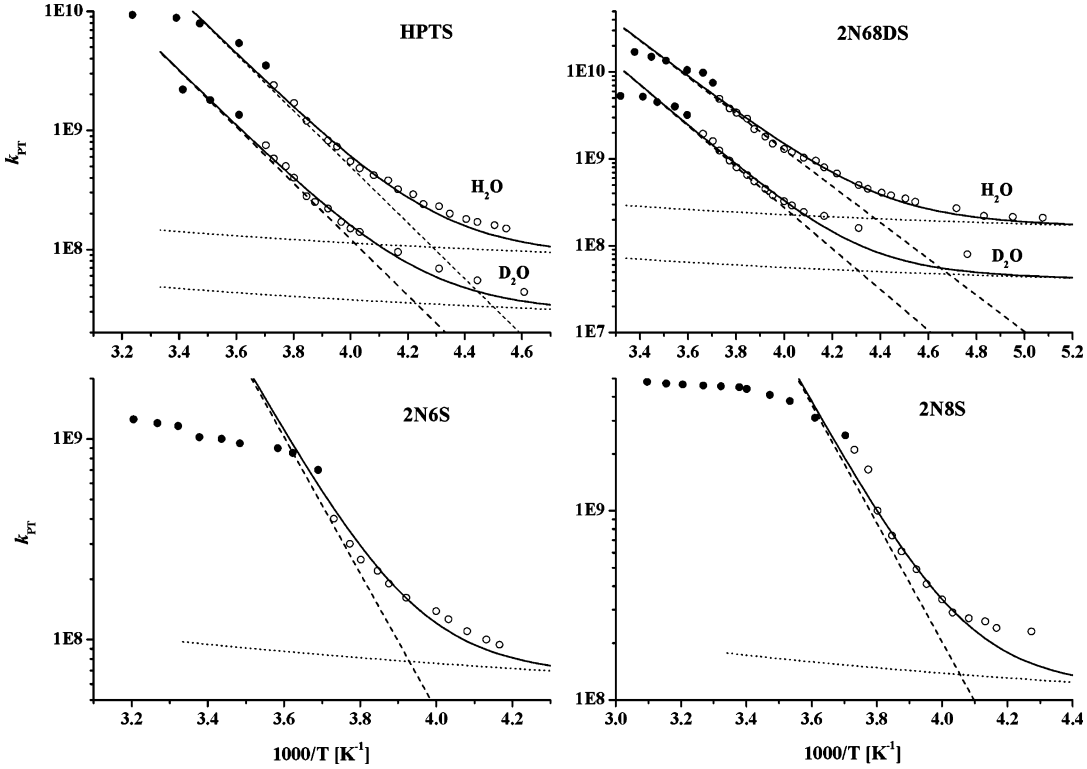

Figure 7. Computer fit of $\ln(k_{PT})$ as a function of $1/T$ using a model combining activated and tunneling proton-transfer process.

hand, the Weller expression for the k_{PT} given in eq 4 does not include the GR contribution to the steady-state ROH and the RO^- fluorescence band intensity. It increases the ROH emission band intensity and decreases the RO^- fluorescence. The neglection of the GR term causes the large decrease of $\ln(\Phi'/\Phi)$ versus $1/T$ seen in Figure 6 at intermediate and low temperatures $T <$ 230 K. The change in the ratio Φ'/Φ from the high temperature 300 K, to the low temperature ~180 K, is by 4 orders of magnitude. The slope of the plot is not constant. In the intermediate temperature range 220−245 K, the slope is smaller than at either higher or lower temperatures. For ice at the high-temperature range $270 > T > 220$ K, we found from the time-resolved emission that the proton-transfer rate does not follow only an activated process. The slope of the plot of $\ln(k_{PT})$ versus $1/T$ decreases as the temperature decreases. We explain this behavior as arising from two mechanisms of the proton transfer; over the barrier dominates in the high-temperature range $270 > T > 245$ K, and proton tunneling prevails at $T \leq 230$ K. At temperatures below 220 K, the slope of the plot of Figure 6 increases. In this range, the proton-transfer process is controlled by the polarization dynamics of the ice medium. Probably the main contribution is that of the hydrogen atom rotation.

In the past, we used a vibrational assisted proton tunneling theory to explain and calculate the temperature dependence of proton transfer of several systems. Trakhtenberg and co-workers developed a simple expression for the temperature dependence of the proton-transfer rate assisted by an intermolecular vibration.[36] For a one-dimensional potential surface with a single intermolecular vibration, Trakhtenberg and co-workers derived a simple formula for the proton-transfer rate constant

$$k(T) = \nu \exp\left(-J(R_0) + \frac{1}{8}(\partial J/\partial R_{0-0})^2 [\delta_{0-0}{}^2]\coth(\hbar\Omega_0/4k_BT)\right) \quad (5)$$

$$J(R) = 2S(R)/\hbar = 2/\hbar \int 2m_H[U(x, R) - E_H(R)]^{1/2}\,dx \quad (6)$$

where ν is the frequency prefactor (of the order of magnitude 10^{13} s^{-1}), Ω_0 is the effective intermolecular frequency, δ_{0-0} is the total amplitude of the zero level oscillations, k_B is the Boltzman constant, and T is the temperature. $J(R)$, the tunneling integral, determines the transparency of the potential barrier of tunneling: it equals twice the classical action $S(R)$ for the hydrogen atom in the underbarrier interval between the turning points. $E_H(R)$ and $U(x, R)$ are the total and potential energy of the tunneling atom, respectively, depending on the distance R between reactants (O---O). R_0 is the equilibrium distance.

In using eq 5 to fit the experimental data, there are several parameters which need to be determined either by the best fit to the experimental data or by acceptable literature values. The pre-exponential factor, ν, has accepted values in the range $10^{13} < \nu < 10^{14}$ s^{-1}. The $^1/_8(\partial J/\partial R_{0-0})^2[\delta_{0-0}{}^2]$ term can be evaluated by the following procedure: the temperature-dependent part of eq 5 is given by the second term of the exponent. Using some manipulation, we get eq 7, which contains only the temperature dependence part of eq 5

$$\ln(k(t)/k(0)) = \frac{1}{8}(\partial J/\partial R_{0-0})^2[\delta_{0-0}{}^2]\{\coth(\hbar\Omega/4k_BT) - 1\} \quad (7)$$

Equation 7 can be used to get both the intermolecular frequency, Ω, and the term $^1/_8(\partial J/\partial R_{0-0})^2[\delta_{0-0}{}^2]$, by fitting it to the experimental data.

Trakhtenberg used a detailed theoretical analysis to fit both the pressure and temperature dependence of proton transfer in flourene−acridine crystal. They estimated the square of the amplitude to be $\delta_{C-N}{}^2 = 0.005$.

Figure 7 shows the Arrhenius plot of the experimental values of $\ln(k_{PT})$ as a function of 1/T and the best calculated fit to the experimental data using two contributions to the proton-transfer rate, the tunneling process (eq 5) and a contribution of an activated process. We get a good fit only when we combine the two contributions to the proton transfer. At high temperature,

TABLE 1: Fitting Parameters of the Proton-Transfer Geminate Recombination Model for HPTS in Water Solution

T (K)	k_{PT}[a] (10^9 s^{-1})	k_r[a,b] (10^9 Å s^{-1})	D[c] (cm^2 s^{-1})	R_D[d] (Å)
296	8.8	5.0	1.0×10^{-4}	28.0
288	7.9	3.3	6.5×10^{-5}	27.5
277	5.4	2.8	5.5×10^{-5}	27.0
270	3.5	2.3	4.4×10^{-5}	26.5
268	2.4	1.5	2.3×10^{-5} [c]	26.2
263	1.7	1.2	1.8×10^{-5} [c]	26.0
260	1.2	0.92	1.5×10^{-5} [c]	26.0
255	0.82	0.90	1.2×10^{-5} [c]	26.0
253	0.73	0.90	1.2×10^{-5} [c]	26.0
250	0.55	0.85	1.2×10^{-5} [c]	26.0
248	0.48	0.85	1.2×10^{-5} [c]	26.0
245	0.42	0.85	1.2×10^{-5} [c]	26.0
242	0.38	0.85	1.2×10^{-5} [c]	26.0
240	0.32	0.85	1.2×10^{-5} [c]	26.0
237	0.29	0.85	1.2×10^{-5} [c]	26.0
235	0.24	0.85	1.2×10^{-5} [c]	26.0
232	0.23	0.85	1.2×10^{-5} [c]	26.0
230	0.20	0.85	1.2×10^{-5} [c]	26.0
227	0.18	0.85	1.2×10^{-5} [c]	26.0
225	0.17	0.85	1.2×10^{-5} [c]	26.0

[a] k_{PT} and k_r are obtained from the fit of the experimental data by the GR model (see text): $\tau^{-1}_{ROH} = 0.18$ ns^{-1}, $\tau^{-1}_{RO^-} = 0.185$ ns^{-1}. [b] The error in the determination of k_r is 50%, see text. [c] Free adjustable parameter. [d] Debye radius $R_D = (Z_1Z_2e^2)/(\epsilon k_B T)$.

TABLE 2: Fitting Parameters of the Proton-Transfer Geminate Recombination Model for 2N68DS in Water Solution

T (K)	k_{PT}[a] (10^9 s^{-1})	k_r[a,b] (10^9 Å s^{-1})	D[c] (cm^2 s^{-1})	R_D[d] (Å)
296	17.0	17	1.0×10^{-4}	21.0
290	15.0	16	9.7×10^{-5}	20.5
285	13.5	15	9.5×10^{-5}	20.0
278	10.5	14.1	8.5×10^{-5}	19.5
273	9.8	12.5	8.0×10^{-5} [c]	18.5
270	7.5	12	7.5×10^{-5} [c]	18.0
268	4.9	9.5	4.5×10^{-5} [c]	17.5
265	3.8	8.3	3.5×10^{-5} [c]	17.5
263	3.4	7.7	2.9×10^{-5} [c]	17.5
260	2.9	7.2	2.5×10^{-5} [c]	17.5
258	2.2	5.1	1.6×10^{-5} [c]	17.5
255	1.8	4.3	1.5×10^{-5} [c]	17.5
253	1.5	4.0	1.3×10^{-5} [c]	17.5
250	1.3	3.2	1.0×10^{-5} [c]	17.5
248	1.2	2.9	1.0×10^{-5} [c]	17.5
245	1.03	2.3	9.7×10^{-6} [c]	19.5
242	0.95	2.3	9.3×10^{-6} [c]	19.5
240	0.80	2.3	8.7×10^{-6} [c]	19.5
237	0.68	2.4	8.0×10^{-6} [c]	19.5
232	0.50	2.4	7.0×10^{-6} [c]	19.5
230	0.45	2.4	6.5×10^{-6} [c]	19.5
227	0.41	2.5	6.5×10^{-6} [c]	19.5
225	0.38	2.7	6.2×10^{-6} [c]	19.5
222	0.35	2.8	6.0×10^{-6} [c]	19.5
220	0.32	3.0	5.8×10^{-6} [c]	19.5
212	0.27	3.7	5.0×10^{-6} [c]	19.5
207	0.22	4.2	4.8×10^{-6} [c]	19.5
202	0.22	5.0	4.8×10^{-6} [c]	19.5

[a] k_{PT} and k_r are obtained from the fit of the experimental data by the GR model (see text): $\tau^{-1}_{ROH} = 0.115$ ns^{-1}, $\tau^{-1}_{RO^-} = 0.08$ ns^{-1}. [b] The error in the determination of k_r is 50%, see text. [c] Free adjustable parameter. [d] Debye radius $R_D = (Z_1Z_2e^2)/(\epsilon k_B T)$.

the main process is the activated process. At low temperature, the tunneling process prevails. Tables 1−4 provide the fitting parameters of the GR model for the various photoacids.

In ice at the high-temperature limit (273 K), the slope is large and is temperature dependent, indicating that the proton-transfer process does not only follow the usual constant-slope Arrhenius

TABLE 3: Fitting Parameters of the Proton-Transfer Geminate Recombination Model for 2N6S in Water Solution

T (K)	k_{PT}[a] (10^9 s^{-1})	k_r[a,b] (10^9 Å s^{-1})	D[c] (cm^2 s^{-1})	R_D[d] (Å)
312	1.25	7.0	1.2×10^{-4}	14.6
306	1.20	7.0	1.2×10^{-4}	14.6
301	1.16	6.5	1.1×10^{-4}	14.3
296	1.02	6.5	1.0×10^{-4}	14.2
291	1.00	6.0	1.0×10^{-4}	14.1
287	0.95	5.6	9.5×10^{-5}	14.1
279	0.90	5.5	8.5×10^{-5}	13.9
276	0.85	5.5	8.5×10^{-5}	13.8
271	0.70	5.5	7.5×10^{-5}	13.5
270	0.55	5.5	6.5×10^{-5} [c]	13.2
268	0.40	4.2	4.5×10^{-5} [c]	13.0
265	0.30	3.8	3.5×10^{-5} [c]	13.0
263	0.25	3.5	2.9×10^{-5} [c]	13.0
260	0.22	3.1	2.5×10^{-5} [c]	13.0
258	0.19	2.9	1.6×10^{-5} [c]	13.0
255	0.17	2.2	1.5×10^{-6} [c]	13.0
250	0.14	2.0	1.3×10^{-6} [c]	13.0
248	0.12	1.2	1.0×10^{-6} [c]	13.0
245	0.11	1.0	1.0×10^{-6} [c]	13.0
242	0.10	1.0	1.0×10^{-6} [c]	13.0
240	0.095	0.95	1.0×10^{-6} [c]	13.0

[a] k_{PT} and k_r are obtained from the fit of the experimental data by the GR model (see text): $\tau^{-1}_{ROH} = 0.10$ ns^{-1}, $\tau^{-1}_{RO^-} = 0.088$ ns^{-1}. [b] The error in the determination of k_r is 50%, see text. [c] Free adjustable parameter. [d] Debye radius $R_D = (Z_1Z_2e^2)/(\epsilon k_B T)$.

TABLE 4: Fitting Parameters of the Proton-Transfer Geminate Recombination Model for 2N68DS in D_2O Solution

T (K)	k_{PT}[a] (10^9 s^{-1})	k_r[a,b] (10^9 Å s^{-1})	D[c] (cm^2 s^{-1})	R_D[d] (Å)
301	5.3	6.5	5×10^{-5}	21.0
293	5.2	6.5	3.8×10^{-5}	21.0
288	4.5	5	3×10^{-5}	21.0
282	4	4	2.6×10^{-5}	21.0
278	3.2	3.3	2.5×10^{-5}	21.0
273	1.95	2.9	2.3×10^{-5}	20.0
270	1.6	2.9	2×10^{-5}	20.0
268	1.25	2.7	5×10^{-5}	20.0
265	0.95	2.65	1.95×10^{-5}	20.0
263	0.8	2.55	1.85×10^{-5}	20.0
260	0.65	2.6	1.75×10^{-5}	20.0
258	0.55	2.55	1.60×10^{-5}	20.0
255	0.45	2.55	1.5×10^{-5}	20.0
253	0.38	2.55	1.4×510^{-5}	20.0
250	0.325	2.55	1.4×10^{-5} [c,e]	20.0
248	0.27	2.55	1.3×10^{-5} [c,e]	20.0
245	0.245	2.55	1.2×10^{-5} [c,f]	20.0
240	0.22	2.55	1.1×10^{-5} [c,f]	20.0
232	0.16	2.55	9.5×10^{-6} [c,g]	20.0
210	0.08	2.55	5×10^{-6} [c,g]	20.0

[a] k_{PT} and k_r are obtained from the fit of the experimental data by the GR model (see text): $\tau^{-1}_{ROH} = 0.10$ ns^{-1}, $\tau^{-1}_{RO^-} = 0.075$ ns^{-1}. [b] The error in the determination of k_r is 50%, see text. [c] Free adjustable parameter. [d] Debye radius $R_D = (Z_1Z_2e^2)/(\epsilon k_B T)$. [e] $\tau^{-1}_{ROH} = 0.11$ ns^{-1}, $\tau^{-1}_{RO^-} = 0.073$ ns^{-1}. [f] $\tau^{-1}_{ROH} = 0.105$ ns^{-1}, $\tau^{-1}_{RO^-} = 0.073$ ns^{-1}. [g] $\tau^{-1}_{ROH} = 0.095$ ns^{-1}, $\tau^{-1}_{RO^-} = 0.073$ ns^{-1}.

behavior. We tried to fit the experimental data only with the vibration-assisted tunneling model (eq 5). We found that the fit is only good at temperatures in the intermediate range $255 > T \geq 220$ K. The plot clearly shows that at low temperatures the rate constant exhibits a smaller temperature dependence.

The fitting parameters for the combined contributions of the tunneling model and activated process for HPTS in H_2O are $\omega = 220$ cm^{-1}, $J(R_o) = 12.2$, and $J'(R) = 18$, $\nu = 10^{13}$ s^{-1}. The activated process parameters are $E_a = 40$kJ/mol and the pre-exponential factor 10^{16} s^{-1}. As seen in Figure 7, the fit using two contributions of over and under the barrier proton-transfer

mechanism is good within a large temperature range while it fails to fit the very high temperatures close to the melting point (273 K). Using the same value of the intermolecular vibration amplitude for δ_{0-0}^2, for all four photoacids we get the same value $J' = 18$ Å^{-1}. The activated process parameters depend on the photoacid strength. The stronger the photoacid is, the lower the activation energy.

As the temperature decreases, the proton transfer by tunneling is more pronounced. The proton tunneling is probably assisted by an intermolecular vibration that modulates the oxygen−oxygen distance between the ROH and the hydrogen-bonded water molecule. Such an intermolecular vibration band with a peak at 229 cm^{-1} is measured in the IR spectrum of ice.[3,37] A concave shape of $\ln(k_{PT})$ versus $1/T$ in the proton-transfer reaction that includes both over the barrier and under the barrier mechanisms was predicted before.[8]

The temperature dependence in the very low-temperature regime $T < 200$ K is not predicted by both proton-transfer mechanisms. Probably in this region the rate-limiting step for a proton-transfer mechanism is the slow solvation dynamics of the hydrogen rotation taking place prior the actual proton-transfer process. This type of a solvent control regime was suggested by us for ESPT in the liquid state.[31,32]

Summary

In this contribution, we studied the temperature dependence of the excited-state proton transfer in ice. Time-resolved emission was employed to measure the photoprotolytic cycle of excited photoacid as a function of temperature, in liquid water and in ice.

As was found previously in the liquid phase, the proton is first transferred from the photoacid to a nearby water molecule. Subsequently, it diffuses in the ice under the influence of the Coulomb potential between H^+ and RO^- that enhances the geminate recombination. We used four photoacids, HPTS and 2-naphtol-6,8-disulfonate (2N68DS), 2N6S and 2N8S. 2N68DS (pK^* ∼ 0.7) is a stronger photoacid than HPTS (pK^* ∼1.35) and transfers a proton to liquid water at about 40 ps, while 2N6S is a weak photoacid (pK ∼ 2) and the proton transfer in liquid water is slow $\tau \approx 900$ ps. In general, all four photoacid results provide similar information on the temperature dependence of k_{PT} in ice.

We find that the proton-transfer rate constant k_{PT} in ice strongly depends on the temperature. We observed three characteristic temperature regions for k_{PT}. In the high-temperature region, $273 > T > 240$ K, the proton-transfer process strongly depends on temperature. In the intermediate temperature range $240 > T > 210$ K, the Arrhenius plot of the rate constant, k_{PT}, exhibits a relatively small temperature dependence. In the low-temperature region $210 < T < 180$ K, the proton-transfer rate depends strongly on the temperature. Below 180 K, we cannot observe the RO^- band in the steady-state emission spectrum of HPTS.

We propose a qualitative model that explains the complex temperature dependence of the proton-transfer rate constant. As in the liquid state,[24] we assume that the reaction in ice can be described by two coordinates: the solvent coordinate and the proton translocation coordinate. The major contribution to the generalized solvent coordinate in ice is the hydrogen rotational motion creating D and L defects. The proton moves to the adjacent hydrogen bonded solvent molecule only when the solvent configuration brings the system to the crossing point. When the solvation dynamics is faster than the proton transfer along the proton coordinate, then the rate-limiting step is the actual proton transfer. This is the case at high and intermediate temperatures. Thus, the temperature dependence of k_{PT} in ice in the high and intermediate temperature range can be explained as arising from contributions of two proton-transfer mechanisms over the barrier and under the barrier. We got a good fit to the temperature dependence of k_{PT} versus $1/T$ in this temperature range. At lower temperature, the rate further decreases because of a limitation on the reaction caused by the solid-state restrictions on the H_2O hydrogen reorientations.

Acknowledgment. We thank Professor N. Agmon and Professor M. Gutman for their helpful and fruitful suggestions and discussions. This work was supported by grants from the Binational U.S.−Israel Science Foundation and the James−Franck German−Israel Program in Laser-Matter Interaction.

References and Notes

(1) Fletcher N.H. In *The Chemical Physics of Ice*; Cambridge University Press: Cambridge, U.K., 1970.

(2) Hobbs. P. V. In *Ice Physics*; Clarendon Press: Oxford, U.K., 1974.

(3) Petrenko, V. F.; Whitworth, R., W. *Physics of Ice*; Oxford University: Oxford, U.K., 1999.

(4) Von Hippel, A.; Runck, A. H.; Westphal, W. B. In *Physics and Chemistry of Ice*; Walley, E., Jones, S. J., Gold, L. W., Eds.; Royal Society of Canada: Ottawa, 1973; p 236.

(5) (a) Eigen, M. *Angew. Chem., Int. Ed. Engl*. **1964**, *3*, 1. (b) Eigen, M.; Kruse, W.; Maass, G.; De Maeyer, L. *Prog. React. Kinet*. **1964**, *2*, 285.

(6) Kelly, I. J.; Salomon, R. R. *J. Chem. Phys.* **1969**, *50*, 75.

(7) Knust, M.; Warman, J. M. *J. Phys. Chem*. **1983**, *87*, 4093.

(8) Bell, R. P. *The Proton in Chemistry*, 2nd ed.; Chapman and Hall: London, 1973.

(9) *Proton Transfer Reaction*; Caldin, E.F., Gold, V., Eds.; Chapman and Hall: London, 1975.

(10) (a) Weller, A. *Prog. React. Kinet.* **1961**, *1*, 189. (b) *Z. Phys. Chem. (Frankfurt am Main)* **1958**, *17*, 224.

(11) Uras-Aytemiz, N.; Joyce, C.; Devlin, J. P. *J. Phys. Chem. A* **2001**, *105*, 10497.

(12) Devlin, J. P.; Gulluru, D.B.; Buch, V. *J. Phys. Chem. B* **2005**, *109*, 3392.

(13) Ireland, J. E.; Wyatt, P. A. *Adv. Phys. Org. Chem.* **1976**, *12*, 131.

(14) (a) Gutman, M.; Nachliel, E. *Biochem. Biophys. Acta* **1990**, *391*, 1015. (b) Pines, E.; Huppert, D. *J. Phys. Chem.* **1983**, *87*, 4471.

(15) Kosower, E. M.; Huppert, D. *Annu. Rev. Phys. Chem.* **1986**, *37*, 127.

(16) Tolbert, L. M.; Solntsev, K. M. *Acc. Chem. Res.* **2002**, *35*, 1.

(17) (a) Rini, M.; Magnes, B. Z.; Pines, E.; Nibbering, E. T. J. *Science* **2003**, *301*, 349. (b) Mohammed, O. F.; Pines, D.; Dreyer, J.; Pines, E.; Nibbering, E. T. J. *Science* **2005**, *310*, 5745.

(18) Prayer, C.; Gustavsson, T.; Tarn-Thi, T. H. In *Fast Elementary Processes in Chemical and Biological Systems*; 54th International Meeting of Physical Chemistry; American Institute of Physics: New York, 1996; p 333.

(19) Tran-Thi, T. H.; Gustavsson, T.; Prayer, C.; Pommeret, S.; Hynes, J. T. *Chem. Phys. Lett.* **2000**, *329*, 421.

(20) Agmon, N. *J. Phys. Chem. A* **2005**, *109*, 13.

(21) Spry, D. B.; Goun, A.; Fayer, M. D. *J. Phys. Chem. A* **2007**, *111*, 230.

(22) *22*) Pines, E., Huppert, D., Agmon, N. *J. Chem. Phys.* **1988**, *88*, 5620.

(23) Agmon, N.; Pines, E.; Huppert, D. *J. Chem. Phys.* **1988**, *88*, 5631.

(24) Cohen, B.; Huppert, D. *J. Phys. Chem. A* **2001**, *105*, 2980−2988.

(25) German, E. D.; Kuznetsov, A. M.; Dogonadze, R. R. *J. Chem. Soc., Faraday Trans. 2* **1980**, *76*, 1128. Ulstrup, J. *Charge-Transfer Processes in Condensed Media*; Springer: Berlin, 1979.

(26) Borgis, D.; Hynes, J. T. *J. Phys. Chem.* **1996**, *100*, 1118.

(27) Poles, E.; Cohen, B.; Huppert, D. *Isr. J. Chem.* **1999**, *39*, 347−360.

(28) Leiderman, P.; Gepshtein, R.; Uritski, A.; Genosar, L.; Huppert, D. *J. Phys. Chem. A* **2006**, *110*, 9039.

(29) Uritski, A.; Leiderman, P.; Huppert, D. *J. Phys. Chem. A* **2006**, *110*, 13686.

(30) Uritski, A.; Leiderman, P.; Huppert D. *J. Phys. Chem. A*, in press.

(31) Cohen, B.; Leiderman, P.; Huppert, D. *J. Phys. Chem. A* **2002**, *106*, 11115.
(32) Cohen, B.; Leiderman, P.; Huppert, D. *J. Lumin.* **2003**, *102*, 676.
(33) Jaccard, C. *Ann. N.Y. Acad. Sci.* **1965**, *125*, 390−400.
(34) Kobayashi, C.; Saito, S.; Ohmine, I. *J. Chem. Phys.*, **2001**, *115*, 4742.
(35) Fraser, R. D. B., Suzuki, E. In *Spectral Analysis*; Blackburn, J. A., Ed.; Marcel Dekker: New York, 1970; p 171.
(36) Trakhtenberg, L. I.; Klochikhin, V. L. *Chem. Phys*. **1998**, *232*, 175.
(37) Bertie, J. E.; Labbe, H. J.; Whalley, E. *J. Chem. Phys.* **1969**, *50*, 4504.